Channel Shaping Using Reconfigurable Intelligent Surfaces: From Diagonal to Beyond

Yang Zhao, *Member, IEEE,* Hongyu Li, *Graduate Student Member, IEEE,*
Massimo Franceschetti, *Fellow, IEEE,* and Bruno Clerckx, *Fellow, IEEE*

***Abstract*—This paper investigates how a passive Reconfigurable Intelligent Surface (RIS) can reshape the Multiple-Input Multiple-Output (MIMO) point-to-point channel in terms of singular values. We depart from the widely-adapted diagonal phase shift model to a general Beyond-Diagonal (BD) architecture, which provides superior shaping capability thanks to in-group connections between elements. An efficient Riemannian Conjugate Gradient (RCG) algorithm is tailored for smooth optimization problems of asymmetric BD-RIS with arbitrary group size, then invoked for the Pareto frontier of channel singular values. To understand the gain from off-diagonal entries, we also derive analytical singular value bounds in Line-of-Sight (LoS) and fully-connected scenarios. As a side product, we tackle MIMO rate maximization problem by alternating between active beamformer (eigenmode transmission) and passive beamformer (RCG algorithm) until convergence. A low-complexity suboptimal solution based on channel shaping is also proposed, where the decoupled problem is formulated as channel power maximization and solved in closed form iteratively. Theoretical analysis and numerical evaluation reveal that the shaping advantage of BD-RIS increases with group size and MIMO dimensions, stemming from stronger subchannel rearrangement and subspace alignment capabilities.**

***Index Terms*—Reconfigurable intelligent surface, multi-input multi-output, manifold optimization, singular value control, rate maximization.**

I. Introduction

Today we are witnessing a paradigm shift from connectivity to intelligence, where the wireless environment is no longer a chaotic medium but a conscious agent that serves on demand. This is empowered by the recent advances in Reconfigurable Intelligent Surface (RIS), a real-time programmable metasurface of numerous non-resonant sub-wavelength scattering elements. It can manipulate the amplitude, phase, frequency, and polarization of the scattered waves [1] with a higher energy efficiency, lower cost, lighter footprint, and greater scalability than relays. Using RIS for passive beamforming has attracted significant interest in wireless communication [2]–[5], backscatter [6], [7], sensing [8], [9], and power transfer literature [10]–[12], reporting a second-order array gain and fourth-order power scaling law (with proper waveform). On the other hand, RIS also enables backscatter modulation by dynamically switching between different patterns, as already investigated [13]–[15] and prototyped [16], [17]. Despite fruitful outcomes, one critical unanswered question is the channel shaping capability: *To what extent can a passive RIS reshape the wireless channel?*

The answer indeed depends on the hardware architecture and scattering model. In conventional (a.k.a. diagonal) RIS, each scattering element is tuned by a dedicated impedance and acts as an *individual* phase shifter [18]. The concept is generalized to Beyond-Diagonal (BD)-RIS [19], [20] which groups adjacent elements using passive components. This allows *cooperative* scattering — wave impinging on one element can propagate within the circuit and depart partially from any element in the same group. BD-RIS can thus control both amplitude and phase of the reflected wave, generalizing the scattering matrix from diagonal with unit-magnitude entries to block diagonal with unitary blocks. Its benefit has been recently shown in receive power maximization [21]–[24], transmit power minimization [25], and rate maximization [24]–[28]. Practical issues such as channel estimation [29] and mutual coupling [30] have also been investigated. Therefore, BD-RIS is envisioned as the next generation channel shaper with stronger signal processing flexibility [31].

Channel shaping is different from passive beamforming as it seeks to modify the inherent properties of the channel itself. This allows one to decouple the RIS-transceiver design and explore the fundamental limits of channel manipulation. For example, diagonal RIS has been proved useful for improving channel power [32], degree of freedom [33], [34], condition number [35], [36], and effective rank [37], [38] in Multiple-Input Multiple-Output (MIMO). In contrast, BD-RIS can provide a higher channel power but existing results are limited to Single-Input Single-Output (SISO)[1]. [21] and Multiple-Input Single-Output (MISO) [22]. While these studies offer promising glimpses into the channel shaping potential, a comprehensive understanding of the capabilities and limitations is desired, and a universal design framework is missing. This paper aims to answer the channel shaping question through theoretical analysis and numerical optimization. The contributions are summarized below.

First, we quantify the capability of a BD-RIS to reshape the MIMO point-to-point channel in terms of singular values. The *Pareto frontiers* are characterized by optimizing the weighted sum of singular values, where the weights can be positive, zero, or negative. The resulting singular value region generalizes most relevant metrics and provides an intuitive channel shaping benchmark. We then discuss some analytical singular value bounds in Line-of-Sight (LoS) and fully-connected scenarios, which help to demystify the gain from off-diagonal entries. This is the first paper to answer the channel shaping question and highlight the BD-RIS gain from a Pareto perspective.

Second, we propose a Riemannian Conjugate Gradient (RCG) algorithm adapted from [39], [40] for smooth optimization problems of asymmetric BD-RIS with arbitrary

[1] In terms of channel shaping, single-stream MIMO with given precoder and combiner [21] is equivalent to SISO.

group size. Specifically, block-wise update is performed along the geodesics[2] of the Stiefel manifold, which are expressed compactly by the exponential map [41]. It features lower complexity and faster convergence than general manifold optimization [42], [43], and solves the Pareto singular value problem. This is the first paper to tailor an efficient optimization framework for asymmetric BD-RIS.

Third, we tackle BD-RIS MIMO rate maximization with two solutions: a local-optimal approach through Alternating Optimization (AO) and a low-complexity approach over channel shaping. The former updates active and passive beamformers by eigenmode transmission and RCG algorithm, respectively. The latter suboptimally decouples both blocks, recasts the shaping problem as channel power maximization, and solves it iteratively in closed form. Interestingly, the gap in between vanishes as BD-RIS evolves from diagonal (single-connected) to unitary (fully-connected). It suggests channel shaping offers a promising low-complexity solution for joint RIS-transceiver designs.

Fourth, extensive simulations reveal that the performance gain from BD-RIS increases with group size and MIMO dimensions. In terms of channel power, fully-connected BD-RIS boosts up to 62%, 312%, 537% over single-connected in 1×1, 4×4, 16×16 MIMO under independent Rayleigh fading, respectively. The superiority stems from stronger *subchannel rearrangement* and *subspace alignment* capabilities empowered by in-group cooperation. It emphasizes the importance of using BD-RIS in large-scale MIMO systems.

Notation: Italic, bold lower-case, and bold upper-case letters indicate scalars, vectors and matrices, respectively. $\jmath$ denotes the imaginary unit. $\mathbb{C}$ represents the set of complex numbers. $\mathbb{U}^{n\times n}$ denotes the set of $n\times n$ unitary matrices. $\mathbf{0}$ and $\mathbf{I}$ are the all-zero and identity matrices with appropriate size, respectively. $\Re\{\cdot\}$ takes the real part of a complex number. $\mathrm{tr}(\cdot)$ and $\det(\cdot)$ evaluates the trace and determinant of a square matrix, respectively. $\mathrm{diag}(\cdot)$ constructs a square matrix with arguments on the main diagonal and zeros elsewhere. $\mathrm{sv}(\cdot)$ returns the singular value vector. $\sigma_n(\cdot)$ and $\lambda_n(\cdot)$ is the n-th largest singular value and eigenvalue, respectively. $(\cdot)^*$, $(\cdot)^\mathsf{T}$, $(\cdot)^\mathsf{H}$, $(\cdot)^\dagger$ $(\cdot)^{(r)}$, $(\cdot)^\star$ denote the conjugate, transpose, conjugate transpose (Hermitian), Moore-Penrose inverse, r-th iterated point, and final solution, respectively. $(\cdot)_{[x:y]}$ is a shortcut for $(\cdot)_x,(\cdot)_{x+1},...,(\cdot)_y$. $|\cdot|$ denotes the absolute value. $\|\cdot\|$ means the Euclidean norm. $\|\cdot\|_\mathrm{F}$ represents the Frobenius norm. $\mathcal{CN}(\mathbf{0},\mathbf{\Sigma})$ is the multivariate Circularly Symmetric Complex Gaussian (CSCG) distribution with mean $\mathbf{0}$ and covariance $\mathbf{\Sigma}$. $\sim$ means "distributed as".

II. BD-RIS Model

Consider a BD-RIS aided point-to-point MIMO system with N_T, N_S, N_R transmit, scatter, and receive antennas, respectively. This configuration is denoted as $N_\mathrm{T}\times N_\mathrm{S}\times N_\mathrm{R}$. The BD-RIS is modeled as an N_S-port network [44] that further divides into G individual groups. Each group contains $L\triangleq N_\mathrm{S}/G$ elements interconnected by real-time reconfigurable components [19]. To simplify the analysis, we assume there are no mutual coupling and the in-group connections can be lossless and asymmetric[3]. The overall scattering matrix is thus block diagonal $\mathbf{\Theta}=\mathrm{diag}(\mathbf{\Theta}_1,...,\mathbf{\Theta}_G)\in\mathbb{U}^{N_\mathrm{S}\times N_\mathrm{S}}$, where $\mathbf{\Theta}_g\in\mathbb{U}^{L\times L}$ is a unitary matrix corresponding to group $g\in\mathcal{G}\triangleq\{1,...,G\}$. Let $\mathbf{H}_\mathrm{D}\in\mathbb{C}^{N_\mathrm{R}\times N_\mathrm{T}}$, $\mathbf{H}_\mathrm{F}\in\mathbb{C}^{N_\mathrm{S}\times N_\mathrm{T}}$, $\mathbf{H}_\mathrm{B}\in\mathbb{C}^{N_\mathrm{R}\times N_\mathrm{S}}$ denote the direct (transmitter-receiver), forward (transmitter-RIS), and backward (RIS-receiver) channels, respectively. The equivalent channel is

$$\mathbf{H}=\mathbf{H}_\mathrm{D}+\mathbf{H}_\mathrm{B}\mathbf{\Theta}\mathbf{H}_\mathrm{F}=\mathbf{H}_\mathrm{D}+\sum_g\mathbf{H}_{\mathrm{B},g}\mathbf{\Theta}_g\mathbf{H}_{\mathrm{F},g}, \tag{1}$$

where $\mathbf{H}_{\mathrm{B},g}\in\mathbb{C}^{N_\mathrm{R}\times L}$ and $\mathbf{H}_{\mathrm{F},g}\in\mathbb{C}^{L\times N_\mathrm{T}}$ are the backward and forward channels of RIS group g, respectively.

Remark 1. *BD-RIS reduces to diagonal RIS and unitary RIS with group size 1 and N_S, respectively.*

Remark 2. *Individual forward and backward Channel State Information (CSI) are required for BD-RIS designs. This is different from diagonal RIS where estimating their product is usually sufficient.*

III. Channel Singular Values Redistribution

A. A Toy Example

We first illustrate the channel shaping capabilities of different RIS by a toy example. Consider a $2\times2\times2$ setup where the direct link is blocked. The diagonal RIS is modeled by $\mathbf{\Theta}_\mathrm{D}=\mathrm{diag}(e^{\jmath\theta_1},e^{\jmath\theta_2})$ while the unitary BD-RIS has 4 independent angular parameters

$$\mathbf{\Theta}_\mathrm{U}=e^{\jmath\phi}\begin{bmatrix} e^{\jmath\alpha}\cos\psi & e^{\jmath\beta}\sin\psi \\ -e^{-\jmath\beta}\sin\psi & e^{-\jmath\alpha}\cos\psi \end{bmatrix}. \tag{2}$$

In particular, ϕ has no impact on the singular value because $\mathrm{sv}(e^{\jmath\phi}\mathbf{A})=\mathrm{sv}(\mathbf{A})$. We also enforce symmetry by $\beta=\pi/2$ such that both architectures have the same number of angular parameters. Fig. 1 shows the channel singular values achieved by an exhaustive grid search over (θ_1,θ_2) for diagonal RIS and (α,ψ) for symmetric unitary RIS. It is observed that both singular values can be manipulated up to 9% using diagonal RIS and 42% using symmetric BD-RIS, despite both architectures have the same number of scattering elements and design parameters. A larger performance gap is expected when asymmetric BD-RIS is available. This example shows BD-RIS can provide a wider dynamic range of channel singular values and motivates further studies on channel shaping.

B. Pareto Frontier Characterization

We then characterize the Pareto frontier of channel singular values by maximizing their weighted sum

$$\max_{\mathbf{\Theta}} \quad \sum_n \rho_n\sigma_n(\mathbf{H}) \tag{3a}$$

$$\text{s.t.} \quad \mathbf{\Theta}_g^\mathsf{H}\mathbf{\Theta}_g=\mathbf{I}, \quad \forall g, \tag{3b}$$

where $n\in\{1,...,\min(N_\mathrm{T},N_\mathrm{R})\}$ and ρ_n is the weight of the n-th singular value that can be positive, zero, or negative. Varying

[2]A geodesic refers to the shortest path between two points in a Riemannian manifold.

[3]While symmetric impedance network is often considered in the literature [19], [21]–[27], asymmetric passive components (e.g., ring hybrids and branch-line hybrids) may also be reconfigured in real time [45]. Asymmetric BD-RIS has been discussed in [20], [27], [28].

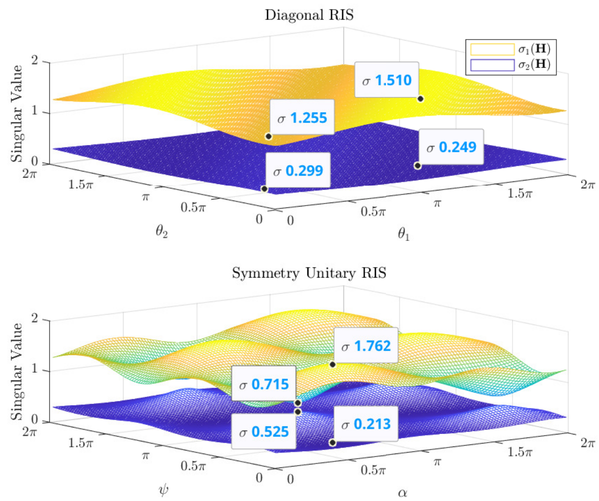

Fig. 1. $2\times2\times2$ (no direct) channel singular value shaping by diagonal and symmetry unitary RIS.

$\{\rho_n\}$ unveils the entire achievable singular value region. Thus, the Pareto frontier problem (3) generalizes most relevant metrics and provides a powerful shaping framework. The objective (3a) is smooth in $\mathbf{\Theta}$ and the feasible domain (3b) for group g corresponds to the Stiefel manifold. Next, we zoom out to general smooth maximization problems of asymmetric BD-RIS.

Inspired by [39], [40], we propose a block-wise RCG algorithm along the geodesics on the Lie group of unitary matrices $\mathbb{U}^{L\times L}$. It leverages the fact that unitary matrices are closed under multiplication. At iteration r, the gradient is computed in the Euclidean space and translated to the Riemannian manifold [42]

$$\nabla_{\mathrm{E},g}^{(r)}=\frac{\partial f(\mathbf{\Theta}_g^{(r)})}{\partial \mathbf{\Theta}_g^{*}}, \tag{4}$$

$$\nabla_{\mathrm{R},g}^{(r)}=\nabla_{\mathrm{E},g}^{(r)}\mathbf{\Theta}_g^{(r)\mathsf{H}}-\mathbf{\Theta}_g^{(r)}\nabla_{\mathrm{E},g}^{(r)\,\mathsf{H}}. \tag{5}$$

The Polak-Ribierre parameter [46] is approximated as [40]

$$\gamma_g^{(r)}=\frac{\operatorname{tr}\big((\nabla_{\mathrm{R},g}^{(r)}-\nabla_{\mathrm{R},g}^{(r-1)})\nabla_{\mathrm{R},g}^{(r)\,\mathsf{H}}\big)}{\operatorname{tr}\big(\nabla_{\mathrm{R},g}^{(r-1)}\nabla_{\mathrm{R},g}^{(r-1)\mathsf{H}}\big)}, \tag{6}$$

and the conjugate direction is

$$\mathbf{D}_g^{(r)}=\nabla_{\mathrm{R},g}^{(r)}+\gamma_g^{(r)}\mathbf{D}_g^{(r-1)}. \tag{7}$$

In the Stiefel manifold, the geodesic emanating from $\mathbf{\Theta}_g^{(r)}$ with velocity $\mathbf{D}_g^{(r)}$ and step size μ is described compactly by the exponential map [41]

$$\mathbf{G}_g^{(r)}(\mu)=\exp(\mu\mathbf{D}_g^{(r)})\mathbf{\Theta}_g^{(r)}. \tag{8}$$

An appropriate $\mu^\star$ can be obtained by the Armijo rule [47].[4] Finally, the scattering matrix is updated along the geodesic as

$$\mathbf{\Theta}_g^{(r+1)}=\mathbf{G}_g^{(r)}(\mu^\star). \tag{9}$$

[4]To double the step size, one only need to square the rotation matrix instead of recomputing the matrix exponential, i.e., $\exp(2\mu\mathbf{D}_g^{(r)})=\exp^2(\mu\mathbf{D}_g^{(r)})$.

Algorithm 1: Block-wise geodesic RCG for asymmetric BD-RIS

Input: $f(\mathbf{\Theta})$, G
Output: $\mathbf{\Theta}^\star$

- **Initialize** $r\leftarrow 0$, $\mathbf{\Theta}^{(0)}$
- **Repeat**
  - **For** $g\leftarrow 1$ to G
    - $\nabla_{\mathrm{E},g}^{(r)}\leftarrow$ (4)
    - $\nabla_{\mathrm{R},g}^{(r)}\leftarrow$ (5)
    - $\gamma_g^{(r)}\leftarrow$ (6)
    - $\mathbf{D}_g^{(r)}\leftarrow$ (7)
    - **If** $\Re\{\operatorname{tr}(\mathbf{D}_g^{(r)\mathsf{H}}\nabla_{\mathrm{R},g}^{(r)})\}<0$ ▷ not an ascent direction
      - $\mathbf{D}_g^{(r)}\leftarrow\nabla_{\mathrm{R},g}^{(r)}$
    - **End If**
    - $\mu\leftarrow 1$
    - $\mathbf{G}_g^{(r)}(\mu)\leftarrow$ (8)
    - **While** $f\big(\mathbf{G}_g^{(r)}(2\mu)\big)-f(\mathbf{\Theta}_g^{(r)})\geq\mu\cdot\operatorname{tr}(\mathbf{D}_g^{(r)}\mathbf{D}_g^{(r)\mathsf{H}})/2$
      - $\mu\leftarrow 2\mu$
    - **End While**
    - **While** $f\big(\mathbf{G}_g^{(r)}(\mu)\big)-f(\mathbf{\Theta}_g^{(r)})<\mu/2\cdot\operatorname{tr}(\mathbf{D}_g^{(r)}\mathbf{D}_g^{(r)\mathsf{H}})/2$
      - $\mu\leftarrow\mu/2$
    - **End While**
    - $\mathbf{\Theta}_g^{(r+1)}\leftarrow$ (9)
  - **End For**
  - $r\leftarrow r+1$
- **Until** $|f(\mathbf{\Theta}^{(r)})-f(\mathbf{\Theta}^{(r-1)})|/f(\mathbf{\Theta}^{(r-1)})\leq\epsilon$

Algorithm 1 summarizes the proposed block-wise geodesic RCG method for smooth maximization problems of asymmetric BD-RIS. Convergence to stationary points is guaranteed.

Remark 3. *Compared with universal manifold optimization [42], [43], Algorithm 1 inherits a trifold benefit from [39], [40]:*

1) *No retraction thanks to rotational update (8), (9);*
2) *Lower computational complexity per iteration;*
3) *Faster convergence thanks to proper parameter space.*

Lemma 1. *The Euclidean gradient of* (3a) *w.r.t. BD-RIS group g is*

$$\frac{\partial\sum_n\rho_n\sigma_n(\mathbf{H})}{\partial\mathbf{\Theta}_g^{*}}=\mathbf{H}_{\mathrm{B},g}^{\mathsf{H}}\mathbf{U}\operatorname{diag}(\rho_1,\ldots,\rho_N)\mathbf{V}^{\mathsf{H}}\mathbf{H}_{\mathrm{F},g}^{\mathsf{H}}, \tag{10}$$

where $\mathbf{U}\in\mathbb{C}^{N_\mathrm{R}\times N}$ and $\mathbf{V}\in\mathbb{C}^{N_\mathrm{T}\times N}$ are the left and right compact singular matrices of $\mathbf{H}$, respectively.

Proof. Let $\mathbf{H}=\sum_n\mathbf{u}_n\sigma_n\mathbf{v}_n^{\mathsf{H}}$ be the compact Singular Value Decomposition (SVD) of the equivalent channel. Since the singular vectors are orthonormal, the n-th singular value can be expressed as

$$\sigma_n=\mathbf{u}_n^{\mathsf{H}}\mathbf{H}\mathbf{v}_n=\mathbf{u}_n^{\mathsf{T}}\mathbf{H}^{*}\mathbf{v}_n^{*}, \tag{11}$$

whose differential w.r.t. $\mathbf{\Theta}_g^{*}$ is

$$\begin{aligned}
\partial\sigma_n&=\partial\mathbf{u}_n^{\mathsf{T}}\underbrace{\mathbf{H}^{*}\mathbf{v}_n^{*}}_{\sum_m\mathbf{u}_m^{*}\sigma_m\mathbf{v}_m^{\mathsf{T}}\mathbf{v}_n}+\mathbf{u}_n^{\mathsf{T}}\cdot\partial\mathbf{H}^{*}\cdot\mathbf{v}_n^{*}+\underbrace{\mathbf{u}_n^{\mathsf{T}}\mathbf{H}^{*}}_{\mathbf{u}_n^{\mathsf{T}}\sum_m\mathbf{u}_m^{*}\sigma_m\mathbf{v}_m^{\mathsf{T}}}\partial\mathbf{v}_n^{*}\\
&=\underbrace{\partial\mathbf{u}_n^{\mathsf{T}}\mathbf{u}_n^{*}}_{\partial 1=0}\cdot\sigma_n+\mathbf{u}_n^{\mathsf{T}}\cdot\partial\mathbf{H}^{*}\cdot\mathbf{v}_n^{*}+\sigma_n\cdot\underbrace{\mathbf{v}_n^{\mathsf{T}}\partial\mathbf{v}_n^{*}}_{\partial 1=0}\\
&=\mathbf{u}_n^{\mathsf{T}}\mathbf{H}_{\mathrm{B},g}^{*}\cdot\partial\mathbf{\Theta}_g^{*}\cdot\mathbf{H}_{\mathrm{F},g}^{*}\mathbf{v}_n^{*}\\
&=\operatorname{tr}(\mathbf{H}_{\mathrm{F},g}^{*}\mathbf{v}_n^{*}\mathbf{u}_n^{\mathsf{T}}\mathbf{H}_{\mathrm{B},g}^{*}\cdot\partial\mathbf{\Theta}_g^{*}).
\end{aligned}$$

According to [48], the corresponding complex derivative is

$$\frac{\partial \sigma_n}{\partial \mathbf{\Theta}_g^*} = \mathbf{H}_{\mathrm{B},g}^{\mathsf{H}} \mathbf{u}_n \mathbf{v}_n^{\mathsf{H}} \mathbf{H}_{\mathrm{F},g}^{\mathsf{H}}. \tag{12}$$

Linear combination of (12) yields (10). □

Algorithm 1 can thus be invoked for the Pareto singular value problem (3) where line 4 uses (10) explicitly.

C. Some Analytical Bounds

We then discuss some analytical bounds related to channel singular values.

Proposition 1 (rank-deficient channel)**.** *In point-to-point MIMO, BD-RIS cannot achieve a higher Degree of Freedom (DoF) than diagonal RIS.*

Proof. The scattering matrix of BD-RIS can be decomposed as[5]

$$\mathbf{\Theta} = \mathbf{L} \mathbf{\Theta}_{\mathrm{D}} \mathbf{R}^{\mathsf{H}}, \tag{13}$$

where $\mathbf{\Theta}_{\mathrm{D}} \in \mathbb{U}^{N_{\mathrm{S}} \times N_{\mathrm{S}}}$ corresponds to diagonal RIS and $\mathbf{L},\mathbf{R} \in \mathbb{U}^{N_{\mathrm{S}} \times N_{\mathrm{S}}}$ are block diagonal matrices of $L \times L$ unitary blocks. Manipulating $\mathbf{L}$ and $\mathbf{R}$ rotates the linear spans of $\bar{\mathbf{H}}_{\mathrm{B}} \triangleq \mathbf{H}_{\mathrm{B}} \mathbf{L}$ and $\bar{\mathbf{H}}_{\mathrm{F}} \triangleq \mathbf{R}^{\mathsf{H}} \mathbf{H}_{\mathrm{F}}$ and maintains their rank. On the other hand, there exists a $\mathbf{\Theta}_{\mathrm{D}}$ such that

$$\begin{aligned}
\mathrm{rank}(\mathbf{H}_{\mathrm{B}} \mathbf{\Theta}_{\mathrm{D}} \mathbf{H}_{\mathrm{F}}) &= \min\big(\mathrm{rank}(\mathbf{H}_{\mathrm{B}}), \mathrm{rank}(\mathbf{\Theta}_{\mathrm{D}}), \mathrm{rank}(\mathbf{H}_{\mathrm{F}})\big) \\
&= \min\big(\mathrm{rank}(\bar{\mathbf{H}}_{\mathrm{B}}), N_{\mathrm{S}}, \mathrm{rank}(\bar{\mathbf{H}}_{\mathrm{F}})\big) \\
&= \max_{\mathbf{\Theta}} \mathrm{rank}(\mathbf{H}_{\mathrm{B}} \mathbf{\Theta} \mathbf{H}_{\mathrm{F}})
\end{aligned}$$

The same result holds if the direct link is present. □

Proposition 2 (LoS forward[6] channel)**.** *If the forward channel is rank-1, then BD-RIS can at most enlarge (resp. suppress) the n-th ($n \geq 2$) channel singular value to the $(n-1)$-th (resp. n-th) singular value of $\mathbf{T}$, that is,*

$$\sigma_1(\mathbf{T}) \geq \sigma_2(\mathbf{H}) \geq \sigma_2(\mathbf{T}) \geq \ldots \geq \sigma_{N-1}(\mathbf{T}) \geq \sigma_N(\mathbf{H}) \geq \sigma_N(\mathbf{T}), \tag{14}$$

where $\mathbf{T}\mathbf{T}^{\mathsf{H}} = \mathbf{H}_{\mathrm{D}}(\mathbf{I} - \mathbf{v}_{\mathrm{F}} \mathbf{v}_{\mathrm{F}}^{\mathsf{H}}) \mathbf{H}_{\mathrm{D}}$ and $\mathbf{v}_{\mathrm{F}}$ is the right compact singular vector of $\mathbf{H}_{\mathrm{F}}$. Note that $\sigma_1(\mathbf{H})$ is unbounded with a sufficiently large RIS.

Proof. Let $\mathbf{H}_{\mathrm{F}} = \sigma_{\mathrm{F}} \mathbf{u}_{\mathrm{F}} \mathbf{v}_{\mathrm{F}}^{\mathsf{H}}$ be the compact SVD of the forward channel. The channel Gram matrix can be written as Hermitian-plus-rank-1:

$$\mathbf{G} \triangleq \mathbf{H}\mathbf{H}^{\mathsf{H}} = \mathbf{Y} + \mathbf{z}\mathbf{z}^{\mathsf{H}}, \tag{15}$$

where $\mathbf{Y} \triangleq \mathbf{H}_{\mathrm{D}}^{\mathsf{H}}(\mathbf{I} - \mathbf{v}_{\mathrm{F}} \mathbf{v}_{\mathrm{F}}^{\mathsf{H}}) \mathbf{H}_{\mathrm{D}}$ and $\mathbf{z} \triangleq \sigma_{\mathrm{F}} \mathbf{H}_{\mathrm{B}} \mathbf{\Theta} \mathbf{u}_{\mathrm{F}} + \mathbf{H}_{\mathrm{D}} \mathbf{v}_{\mathrm{F}}$. By the Cauchy interlacing formula [49], the n-th ($n \geq 2$) eigenvalues of $\mathbf{G}$ are bounded by

$$\lambda_1(\mathbf{Y}) \geq \lambda_2(\mathbf{G}) \geq \lambda_2(\mathbf{Y}) \geq \ldots \geq \lambda_{N-1}(\mathbf{Y}) \geq \lambda_N(\mathbf{G}) \geq \lambda_N(\mathbf{Y}). \tag{16}$$

Since $\mathbf{Y} = \mathbf{T}\mathbf{T}^{\mathsf{H}}$ is positive semi-definite, the eigenvalues are non-negative and taking the square root of (16) gives (14). □

It is worth notice that a similar conclusion holds for diagonal RIS [50]. We will later show that for a finite N_{S}, using a larger group size can approach those bounds better.

[5]This is because (block) unitary matrices are closed under multiplication.
[6]A similar result holds for LoS backward channel.

Proposition 3 (fully-connected RIS without direct link)**.** *If the BD-RIS is fully-connected and the direct link is absent, then*

$$\mathrm{sv}(\mathbf{H}) = \mathrm{sv}(\mathbf{B}\mathbf{F}), \tag{17}$$

where $\mathbf{B}$ and $\mathbf{F}$ are arbitrary matrices with the same singular values as $\mathbf{H}_{\mathrm{B}}$ and $\mathbf{H}_{\mathrm{F}}$, respectively,

Proof. Let $\mathbf{H}_{\mathrm{B}} = \mathbf{U}_{\mathrm{B}} \mathbf{\Sigma}_{\mathrm{B}} \mathbf{V}_{\mathrm{B}}^{\mathsf{H}}$ and $\mathbf{H}_{\mathrm{F}} = \mathbf{U}_{\mathrm{F}} \mathbf{\Sigma}_{\mathrm{F}} \mathbf{V}_{\mathrm{F}}^{\mathsf{H}}$ be the SVD of the backward and forward channels, respectively. The scattering matrix of fully-connected RIS can be decomposed as

$$\mathbf{\Theta} = \mathbf{V}_{\mathrm{B}} \mathbf{X} \mathbf{U}_{\mathrm{F}}^{\mathsf{H}}, \tag{18}$$

where $\mathbf{X} \in \mathbb{U}^{N_{\mathrm{S}} \times N_{\mathrm{S}}}$ is a unitary matrix to be designed. The equivalent channel is thus a function of $\mathbf{X}$

$$\mathbf{H} = \mathbf{H}_{\mathrm{B}} \mathbf{\Theta} \mathbf{H}_{\mathrm{F}} = \mathbf{U}_{\mathrm{B}} \mathbf{\Sigma}_{\mathrm{B}} \mathbf{X} \mathbf{\Sigma}_{\mathrm{F}} \mathbf{V}_{\mathrm{F}}^{\mathsf{H}}. \tag{19}$$

Since $\mathrm{sv}(\mathbf{U}\mathbf{A}\mathbf{V}^{\mathsf{H}}) = \mathrm{sv}(\mathbf{A})$ for unitary $\mathbf{U}$ and $\mathbf{V}$, we have

$$\begin{aligned}
\mathrm{sv}(\mathbf{H}) &= \mathrm{sv}(\mathbf{U}_{\mathrm{B}} \mathbf{\Sigma}_{\mathrm{B}} \mathbf{X} \mathbf{\Sigma}_{\mathrm{F}} \mathbf{V}_{\mathrm{F}}^{\mathsf{H}}) \\
&= \mathrm{sv}(\mathbf{\Sigma}_{\mathrm{B}} \mathbf{X} \mathbf{\Sigma}_{\mathrm{F}}) \\
&= \mathrm{sv}(\bar{\mathbf{U}}_{\mathrm{B}} \mathbf{\Sigma}_{\mathrm{B}} \bar{\mathbf{V}}_{\mathrm{B}}^{\mathsf{H}} \bar{\mathbf{U}}_{\mathrm{F}} \mathbf{\Sigma}_{\mathrm{F}} \bar{\mathbf{V}}_{\mathrm{F}}^{\mathsf{H}}) \\
&= \mathrm{sv}(\mathbf{B}\mathbf{F}),
\end{aligned}$$

where $\bar{\mathbf{U}}_{\mathrm{B/F}}$ and $\bar{\mathbf{V}}_{\mathrm{B/F}}$ are arbitrary unitary matrices. □

There exist many singular value bounds on the product of two matrices in terms of their own singular values. One comprehensive answer is [51]

$$\prod_{k \in K} \sigma_k(\mathbf{H}) \leq \prod_{i \in I} \sigma_i(\mathbf{H}_{\mathrm{B}}) \prod_{j \in J} \sigma_j(\mathbf{H}_{\mathrm{F}}), \tag{20}$$

for all admissible triples $(I,J,K) \in T_r^n$ with $r < n$, where

$$\begin{aligned}
T_r^n \triangleq \Big\{ &(I,J,K) \in U_r^n \,|\, \forall p < r, (F,G,H) \in T_p^r, \\
&\sum_{f \in F} i_f + \sum_{g \in G} j_g \leq \sum_{h \in H} k_h + p(p+1)/2 \Big\},
\end{aligned} \tag{21}$$

$$U_r^n \triangleq \Big\{ (I,J,K) \,|\, \sum_{i \in I} i + \sum_{j \in J} j = \sum_{k \in K} k + r(r+1)/2 \Big\}. \tag{22}$$

It implies the following special cases:

- upper bound on the largest singular value
$$\sigma_1(\mathbf{H}) \leq \sigma_1(\mathbf{H}_{\mathrm{B}}) \sigma_1(\mathbf{H}_{\mathrm{F}}); \tag{23}$$
- lower bound on the smallest singular value
$$\sigma_N(\mathbf{H}) \geq \sigma_N(\mathbf{H}_{\mathrm{B}}) \sigma_N(\mathbf{H}_{\mathrm{F}}); \tag{24}$$
- upper bound on the product of first k singular values
$$\prod_{n=1}^{k} \sigma_n(\mathbf{H}) \leq \prod_{n=1}^{k} \sigma_n(\mathbf{H}_{\mathrm{B}}) \prod_{n=1}^{k} \sigma_n(\mathbf{H}_{\mathrm{F}}); \tag{25}$$
- lower bound on the product of last k singular values
$$\prod_{n=N}^{N-k+1} \sigma_n(\mathbf{H}) \geq \prod_{n=N}^{N-k+1} \sigma_n(\mathbf{H}_{\mathrm{B}}) \prod_{n=N}^{N-k+1} \sigma_n(\mathbf{H}_{\mathrm{F}}); \tag{26}$$

- upper bound on the sum of first k singular values to the power of $p>0$

$$\sum_{n=1}^{k}\sigma_n^p(\mathbf{H})\leq\sum_{n=1}^{k}\sigma_n^p(\mathbf{H}_\mathrm{B})\sigma_n^p(\mathbf{H}_\mathrm{F}); \tag{27}$$

when $k=N$ and $p=2$, it suggests the channel power is upper bounded by the sum of (sorted) element-wise power product of backward and forward subchannel.

Remark 4. *Interestingly,* (20)–(27) *are simultaneously tight when* $\mathbf{\Theta}=\mathbf{V}_\mathrm{B}\mathbf{U}_\mathrm{F}^\mathsf{H}$. *From* (18) *and* (19)*, we conclude the off-diagonal entries can enhance the capabilities of*

- *subspace alignment:* $\mathbf{V}_\mathrm{B}$ *and* $\mathbf{U}_\mathrm{F}^\mathsf{H}$ *in* (18) *fully align the subspaces of* $\mathbf{H}_\mathrm{B}$ *and* $\mathbf{H}_\mathrm{F}$ *by rotation;*
- *subchannel rearrangement:* $\mathbf{X}=\mathbf{I}$ *in* (19) *pairs the subchannels of* $\mathbf{H}_\mathrm{B}$ *and* $\mathbf{H}_\mathrm{F}$ *from strongest to weakest, which attains the maximal in rearrangement inequality.*

Tight bounds are generally unavailable when MIMO direct link is present. This is because the RIS needs to balance the direct-indirect (additive) and backward-forward (multiplicative) subspace alignments.

IV. Achievable Rate Maximization

The MIMO achievable rate maximization problem is formulated w.r.t. joint active and passive beamforming

$$\max_{\mathbf{W},\mathbf{\Theta}} \quad R=\log\det\left(\mathbf{I}+\frac{\mathbf{W}^\mathsf{H}\mathbf{H}^\mathsf{H}\mathbf{H}\mathbf{W}}{\eta}\right) \tag{28a}$$
$$\text{s.t.} \quad \|\mathbf{W}\|_\mathrm{F}^2\leq P, \tag{28b}$$
$$\mathbf{\Theta}_g^\mathsf{H}\mathbf{\Theta}_g=\mathbf{I}, \quad \forall g, \tag{28c}$$

where $\mathbf{W}$ is the transmit precoder, R is the achievable rate, η is the noise power, and P is the transmit power budget. Two methods are proposed below to solve problem (28).

A. Alternating Optimization

Consider an AO approach that updates $\mathbf{\Theta}$ and $\mathbf{W}$ iteratively. For a given $\mathbf{W}$, the passive beamforming subproblem is

$$\max_{\mathbf{\Theta}} \quad \log\det\left(\mathbf{I}+\frac{\mathbf{H}\mathbf{Q}\mathbf{H}^\mathsf{H}}{\eta}\right) \tag{29a}$$
$$\text{s.t.} \quad \mathbf{\Theta}_g^\mathsf{H}\mathbf{\Theta}_g=\mathbf{I}, \quad \forall g, \tag{29b}$$

where $\mathbf{Q}\triangleq\mathbf{W}\mathbf{W}^\mathsf{H}$ is the transmit covariance matrix.

Lemma 2. *The Euclidean gradient of* (29a) *w.r.t. BD-RIS block g is*

$$\frac{\partial R}{\partial\mathbf{\Theta}_g^*}=\frac{1}{\eta}\mathbf{H}_{\mathrm{B},g}^\mathsf{H}\left(\mathbf{I}+\frac{\mathbf{H}\mathbf{Q}\mathbf{H}^\mathsf{H}}{\eta}\right)^{-1}\mathbf{H}\mathbf{Q}\mathbf{H}_{\mathrm{F},g}^\mathsf{H}. \tag{30}$$

Proof. The differential of R w.r.t. $\mathbf{\Theta}_g^*$ is [48]

$$\begin{aligned}\partial R&=\frac{1}{\eta}\mathrm{tr}\left\{\partial\mathbf{H}^*\cdot\mathbf{Q}^\mathsf{T}\mathbf{H}^\mathsf{T}\left(\mathbf{I}+\frac{\mathbf{H}^*\mathbf{Q}^\mathsf{T}\mathbf{H}^\mathsf{T}}{\eta}\right)^{-1}\right\}\\&=\frac{1}{\eta}\mathrm{tr}\left\{\mathbf{H}_{\mathrm{B},g}^*\cdot\partial\mathbf{\Theta}_g^*\cdot\mathbf{H}_{\mathrm{F},g}^*\mathbf{Q}^\mathsf{T}\mathbf{H}^\mathsf{T}\left(\mathbf{I}+\frac{\mathbf{H}^*\mathbf{Q}^\mathsf{T}\mathbf{H}^\mathsf{T}}{\eta}\right)^{-1}\right\}\\&=\frac{1}{\eta}\mathrm{tr}\left\{\mathbf{H}_{\mathrm{F},g}^*\mathbf{Q}^\mathsf{T}\mathbf{H}^\mathsf{T}\left(\mathbf{I}+\frac{\mathbf{H}^*\mathbf{Q}^\mathsf{T}\mathbf{H}^\mathsf{T}}{\eta}\right)^{-1}\mathbf{H}_{\mathrm{B},g}^*\cdot\partial\mathbf{\Theta}_g^*\right\},\end{aligned}$$

and the corresponding complex derivative is (30). □

Algorithm 1 is then invoked to solve problem (28) where line 4 uses (30) explicitly. Since (29a) is a concave function of $\mathbf{\Theta}$, convergence to local-optimal points is guaranteed. On the other hand, the global optimal transmit precoder for a fixed $\mathbf{\Theta}$ is given by the eigenmode transmission [52]

$$\mathbf{W}^\star=\mathbf{V}\mathbf{S}^{\star 1/2}, \tag{31}$$

where $\mathbf{V}$ is the right channel singular matrix and $\mathbf{S}^\star$ is the optimal water-filling power allocation matrix. The overall AO algorithm converges to local-optimal points of problem (28) since each subproblem is solved optimally and the objective is bounded from above.

B. Low-Complexity Solution

We then propose a low-complexity solution to problem (28) based on channel shaping. The passive beamforming subproblem (29) involves transmit covariance matrix $\mathbf{Q}$ and thus requires iterative RCG update. Instead, we decouple the joint RIS-transceiver design by recasting (29) as channel power maximization

$$\max_{\mathbf{\Theta}} \quad \|\mathbf{H}_\mathrm{D}+\mathbf{H}_\mathrm{B}\mathbf{\Theta}\mathbf{H}_\mathrm{F}\|_\mathrm{F}^2 \tag{32a}$$
$$\text{s.t.} \quad \mathbf{\Theta}_g^\mathsf{H}\mathbf{\Theta}_g=\mathbf{I}, \quad \forall g. \tag{32b}$$

Remark 5. *As mentioned in Section III-C, the key of solving* (32) *is to balance the additive and multiplicative subspace alignments. Problem* (32) *is very similar (in terms of maximizing the inner product of* $\mathbf{H}_\mathrm{D}$ *and* $\mathbf{H}_\mathrm{B}\mathbf{\Theta}\mathbf{H}_\mathrm{F}$*) to the weighted orthogonal Procrustes problem [53]*

$$\min_{\mathbf{\Theta}} \quad \|\mathbf{H}_\mathrm{D}-\mathbf{H}_\mathrm{B}\mathbf{\Theta}\mathbf{H}_\mathrm{F}\|_\mathrm{F}^2 \tag{33a}$$
$$\text{s.t.} \quad \mathbf{\Theta}^\mathsf{H}\mathbf{\Theta}=\mathbf{I}, \tag{33b}$$

which has no trivial solution. One lossy transformation, by moving $\mathbf{\Theta}$ *to one side [54], formulates standard orthogonal Procrustes problems*

$$\min_{\mathbf{\Theta}} \quad \|\mathbf{H}_\mathrm{B}^\dagger\mathbf{H}_\mathrm{D}-\mathbf{\Theta}\mathbf{H}_\mathrm{F}\|_\mathrm{F}^2 \text{ or } \|\mathbf{H}_\mathrm{D}\mathbf{H}_\mathrm{F}^\dagger-\mathbf{H}_\mathrm{B}\mathbf{\Theta}\|_\mathrm{F}^2 \tag{34a}$$
$$\text{s.t.} \quad \mathbf{\Theta}^\mathsf{H}\mathbf{\Theta}=\mathbf{I}, \tag{34b}$$

which has global optimal solutions $\mathbf{\Theta}^\star=\mathbf{U}\mathbf{V}^\mathsf{H}$ *where* $\mathbf{U}$ *and* $\mathbf{V}$ *are the left and right singular matrices of* $\mathbf{H}_\mathrm{B}^\dagger\mathbf{H}_\mathrm{D}\mathbf{H}_\mathrm{F}^\mathsf{H}$ *or* $\mathbf{H}_\mathrm{B}^\mathsf{H}\mathbf{H}_\mathrm{D}\mathbf{H}_\mathrm{F}^\dagger$ *[49]. This naive solution will be compared with the one proposed below.*

Inspired by [55], we successively approximate the quadratic objective (32a) by local Taylor expansions and solve each iteration in closed form.

Proposition 4. *Start from any* $\mathbf{\Theta}^{(0)}\in\mathbb{U}^{N_\mathrm{S}\times N_\mathrm{S}}$*, the sequence*

$$\mathbf{\Theta}_g^{(r+1)}=\mathbf{U}_g^{(r)}\mathbf{V}_g^{(r)}, \quad \forall g \tag{35}$$

converges to a stationary point of (32)*, where* $\mathbf{U}_g^{(r)}$ *and* $\mathbf{V}_g^{(r)}$ *are the left and right compact singular matrix of*

$$\mathbf{M}_g^{(r)}=\mathbf{H}_{\mathrm{B},g}^\mathsf{H}\left(\mathbf{H}_\mathrm{D}+\mathbf{H}_\mathrm{B}\mathrm{diag}\left(\mathbf{\Theta}_{[1:g-1]}^{(r+1)},\mathbf{\Theta}_{[g:G]}^{(r)}\right)\mathbf{H}_\mathrm{F}\right)\mathbf{H}_{\mathrm{F},g}^\mathsf{H} \tag{36}$$

$$2\Re\Big\{\sum_g \mathrm{tr}(\tilde{\mathbf{\Theta}}_g^{\mathsf{H}}\mathbf{H}_{\mathrm{B},g}^{\mathsf{H}}\mathbf{H}_{\mathrm{D}}\mathbf{H}_{\mathrm{F},g}^{\mathsf{H}})+\sum_{g_1,g_2}\mathrm{tr}(\tilde{\mathbf{\Theta}}_{g_1}^{\mathsf{H}}\mathbf{H}_{\mathrm{B},g_1}^{\mathsf{H}}\mathbf{H}_{\mathrm{B},g_2}\mathbf{\Theta}_{g_2}\mathbf{H}_{\mathrm{F},g_2}\mathbf{H}_{\mathrm{F},g_1}^{\mathsf{H}})\Big\}\geq 2\Re\Big\{\sum_g \mathrm{tr}(\mathbf{\Theta}_g^{\mathsf{H}}\mathbf{H}_{\mathrm{B},g}^{\mathsf{H}}\mathbf{H}_{\mathrm{D}}\mathbf{H}_{\mathrm{F},g}^{\mathsf{H}})+\sum_{g_1,g_2}\mathrm{tr}(\mathbf{\Theta}_{g_1}^{\mathsf{H}}\mathbf{H}_{\mathrm{B},g_1}^{\mathsf{H}}\mathbf{H}_{\mathrm{B},g_2}\mathbf{\Theta}_{g_2}\mathbf{H}_{\mathrm{F},g_2}\mathbf{H}_{\mathrm{F},g_1}^{\mathsf{H}})\Big\} \quad (41)$$

$$\sum_{g_1,g_2}\mathrm{tr}(\mathbf{H}_{\mathrm{F},g_1}^{\mathsf{H}}\tilde{\mathbf{\Theta}}_{g_1}^{\mathsf{H}}\mathbf{H}_{\mathrm{B},g_1}^{\mathsf{H}}\mathbf{H}_{\mathrm{B},g_2}\tilde{\mathbf{\Theta}}_{g_2}\mathbf{H}_{\mathrm{F},g_2})-2\Re\Big\{\sum_{g_1,g_2}\mathrm{tr}(\mathbf{H}_{\mathrm{F},g_1}^{\mathsf{H}}\tilde{\mathbf{\Theta}}_{g_1}^{\mathsf{H}}\mathbf{H}_{\mathrm{B},g_1}^{\mathsf{H}}\mathbf{H}_{\mathrm{B},g_2}\mathbf{\Theta}_{g_2}\mathbf{H}_{\mathrm{F},g_2})\Big\}+\sum_{g_1,g_2}\mathrm{tr}(\mathbf{H}_{\mathrm{F},g_1}^{\mathsf{H}}\mathbf{\Theta}_{g_1}^{\mathsf{H}}\mathbf{H}_{\mathrm{B},g_1}^{\mathsf{H}}\mathbf{H}_{\mathrm{B},g_2}\mathbf{\Theta}_{g_2}\mathbf{H}_{\mathrm{F},g_2})\geq 0 \quad (42)$$

Proof. The differential of (32a) w.r.t. $\mathbf{\Theta}_g^*$ is

$$\begin{aligned}\partial\|\mathbf{H}\|_{\mathrm{F}}^2 &= \mathrm{tr}\big(\mathbf{H}_{\mathrm{B},g}^*\cdot\partial\mathbf{\Theta}_g^*\cdot\mathbf{H}_{\mathrm{F},g}^*(\mathbf{H}_{\mathrm{D}}^{\mathsf{T}}+\mathbf{H}_{\mathrm{F}}^{\mathsf{T}}\mathbf{\Theta}^{\mathsf{T}}\mathbf{H}_{\mathrm{B}}^{\mathsf{T}})\big)\\ &= \mathrm{tr}\big(\mathbf{H}_{\mathrm{F},g}^*(\mathbf{H}_{\mathrm{D}}^{\mathsf{T}}+\mathbf{H}_{\mathrm{F}}^{\mathsf{T}}\mathbf{\Theta}^{\mathsf{T}}\mathbf{H}_{\mathrm{B}}^{\mathsf{T}})\mathbf{H}_{\mathrm{B},g}^*\cdot\partial\mathbf{\Theta}_g^*\big)\end{aligned}$$

and the corresponding complex derivative is

$$\frac{\partial\|\mathbf{H}\|_{\mathrm{F}}^2}{\partial\mathbf{\Theta}_g^*}=\mathbf{H}_{\mathrm{B},g}^{\mathsf{H}}(\mathbf{H}_{\mathrm{D}}+\mathbf{H}_{\mathrm{B}}\mathbf{\Theta}\mathbf{H}_{\mathrm{F}})\mathbf{H}_{\mathrm{F},g}^{\mathsf{H}}=\mathbf{M}_g. \quad (37)$$

First, we approximate the quadratic objective (32a) by its local Taylor expansion

$$\max_{\mathbf{\Theta}} \quad \sum_g 2\Re\big\{\mathrm{tr}(\mathbf{\Theta}_g^{\mathsf{H}}\mathbf{M}_g)\big\} \quad (38a)$$

$$\text{s.t.} \quad \mathbf{\Theta}_g^{\mathsf{H}}\mathbf{\Theta}_g=\mathbf{I}, \quad \forall g. \quad (38b)$$

Let $\mathbf{M}_g=\mathbf{U}_g\mathbf{\Sigma}_g\mathbf{V}_g^{\mathsf{H}}$ be the compact SVD of $\mathbf{M}_g$. We have

$$\Re\big\{\mathrm{tr}(\mathbf{\Theta}_g^{\mathsf{H}}\mathbf{M}_g)\big\}=\Re\big\{\mathrm{tr}(\mathbf{\Sigma}_g\mathbf{V}_g^{\mathsf{H}}\mathbf{\Theta}_g^{\mathsf{H}}\mathbf{U}_g)\big\}\leq\mathrm{tr}(\mathbf{\Sigma}_g). \quad (39)$$

The upper bound is tight when $\mathbf{V}_g^{\mathsf{H}}\mathbf{\Theta}_g^{\mathsf{H}}\mathbf{U}_g=\mathbf{I}$, which implies the optimal solution of (38) is $\tilde{\mathbf{\Theta}}_g=\mathbf{U}_g\mathbf{V}_g^{\mathsf{H}}$, $\forall g$.

Next, we prove that solving (38) successively does not decrease (32a). Since $\tilde{\mathbf{\Theta}}$ optimal for problem (38), we have $\sum_g 2\Re\{\mathrm{tr}(\tilde{\mathbf{\Theta}}_g^{\mathsf{H}}\mathbf{M}_g)\}\geq\sum_g 2\Re\{\mathrm{tr}(\mathbf{\Theta}_g^{\mathsf{H}}\mathbf{M}_g)\}$ which is explicitly expressed by (41). On the other hand, expanding $\|\sum_g\mathbf{H}_{\mathrm{B},g}\tilde{\mathbf{\Theta}}_g\mathbf{H}_{\mathrm{F},g}-\sum_g\mathbf{H}_{\mathrm{B},g}\mathbf{\Theta}_g\mathbf{H}_{\mathrm{F},g}\|_{\mathrm{F}}^2\geq 0$ gives (42). Adding (41) and (42), we have

$$\begin{aligned}&2\Re\Big\{\mathrm{tr}(\tilde{\mathbf{\Theta}}^{\mathsf{H}}\mathbf{H}_{\mathrm{B}}^{\mathsf{H}}\mathbf{H}_{\mathrm{D}}\mathbf{H}_{\mathrm{F}}^{\mathsf{H}})\Big\}+\mathrm{tr}(\mathbf{H}_{\mathrm{F}}^{\mathsf{H}}\tilde{\mathbf{\Theta}}^{\mathsf{H}}\mathbf{H}_{\mathrm{B}}^{\mathsf{H}}\mathbf{H}_{\mathrm{B}}\tilde{\mathbf{\Theta}}\mathbf{H}_{\mathrm{F}})\\ &\geq 2\Re\Big\{\mathrm{tr}(\mathbf{\Theta}^{\mathsf{H}}\mathbf{H}_{\mathrm{B}}^{\mathsf{H}}\mathbf{H}_{\mathrm{D}}\mathbf{H}_{\mathrm{F}}^{\mathsf{H}})\Big\}+\mathrm{tr}(\mathbf{H}_{\mathrm{F}}^{\mathsf{H}}\mathbf{\Theta}^{\mathsf{H}}\mathbf{H}_{\mathrm{B}}^{\mathsf{H}}\mathbf{H}_{\mathrm{B}}\mathbf{\Theta}\mathbf{H}_{\mathrm{F}}), \quad (40)\end{aligned}$$

which confirms that updating $\tilde{\mathbf{\Theta}}$ does not decrease (32a).

Finally, we prove that the converging point of (38), denoted by $\tilde{\mathbf{\Theta}}^?$, is a stationary point of (32). The Karush-Kuhn-Tucker (KKT) conditions of (32) and (38) are equivalent in terms of primal/dual feasibility and complementary slackness, while the stationary conditions are respectively, $\forall g$,

$$\mathbf{H}_{\mathrm{B},g}^{\mathsf{H}}(\mathbf{H}_{\mathrm{D}}+\mathbf{H}_{\mathrm{B}}\mathbf{\Theta}^\star\mathbf{H}_{\mathrm{F}})\mathbf{H}_{\mathrm{F},g}^{\mathsf{H}}-\mathbf{\Theta}_g^\star\mathbf{\Lambda}_g^{\mathsf{H}}=0, \quad (43)$$

$$\mathbf{M}_g-\mathbf{\Theta}_g^\star\mathbf{\Lambda}_g^{\mathsf{H}}=0. \quad (44)$$

On convergence, (44) becomes $\mathbf{H}_{\mathrm{B},g}^{\mathsf{H}}(\mathbf{H}_{\mathrm{D}}+\mathbf{H}_{\mathrm{B}}\mathbf{\Theta}^?\mathbf{H}_{\mathrm{F}})\mathbf{H}_{\mathrm{F},g}^{\mathsf{H}}-\mathbf{\Theta}_g^?\mathbf{\Lambda}_g^{\mathsf{H}}=0$ and reduces to (43). The proof is completed. □

Once the channel shaping problem (32) is solved, the transmit precoder can be obtained by (31). This two-stage approach decouples both blocks and is computationally efficient.

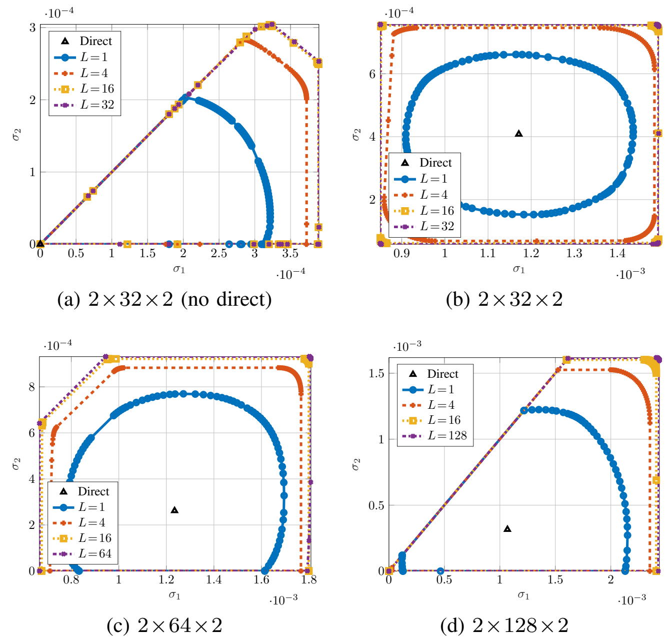

(a) $2\times 32\times 2$ (no direct)

(b) $2\times 32\times 2$

(c) $2\times 64\times 2$

(d) $2\times 128\times 2$

Fig. 2. Pareto frontiers of channel singular values reshaped by BD-RIS.

V. Simulation Results

In this section, we provide numerical results to evaluate the proposed BD-RIS designs. Consider a distance-dependent path loss model $\Lambda(d)=\Lambda_0 d^{-\gamma}$ where Λ_0 is the reference path loss at distance 1 m, d is the propagation distance, and γ is the path loss exponent. The small-scale fading model is $\mathbf{H}=\sqrt{\kappa/(1+\kappa)}\mathbf{H}_{\mathrm{LoS}}+\sqrt{1/(1+\kappa)}\mathbf{H}_{\mathrm{NLoS}}$, where κ is the Rician K-factor, $\mathbf{H}_{\mathrm{LoS}}$ is the deterministic LoS component, and $\mathbf{H}_{\mathrm{NLoS}}\sim\mathcal{CN}(\mathbf{0},\mathbf{I})$ is the Rayleigh component. We set $\Lambda_0=-30$dB, $d_{\mathrm{D}}=14.7$m, $d_{\mathrm{F}}=10$m, $d_{\mathrm{B}}=6.3$m, $\gamma_{\mathrm{D}}=3$, $\gamma_{\mathrm{F}}=2.4$ and $\gamma_{\mathrm{B}}=2$ for reference, which corresponds to a typical indoor environment with $\Lambda_{\mathrm{D}}=-65$dB, $\Lambda_{\mathrm{F}}=-54$dB, $\Lambda_{\mathrm{B}}=-46$dB. The indirect path via RIS is thus 35 dB weaker than the direct path. Rayleigh fading is assumed for all channels $\kappa_{\mathrm{D}},\kappa_{\mathrm{B}},\kappa_{\mathrm{F}}\to\infty$ unless otherwise specified.

A. Channel Singular Values Redistribution

The Pareto singular value frontiers of a 2×2 MIMO with a 32-element BD-RIS is shown in Fig. 2.

B. Achievable Rate Maximization

References

[1] E. Basar, M. D. Renzo, J. D. Rosny, M. Debbah, M.-S. Alouini, and R. Zhang, "Wireless communications through reconfigurable intelligent surfaces," *IEEE Access*, vol. 7, pp. 116 753–116 773, 2019. [Online]. Available: https://ieeexplore.ieee.org/document/8796365/

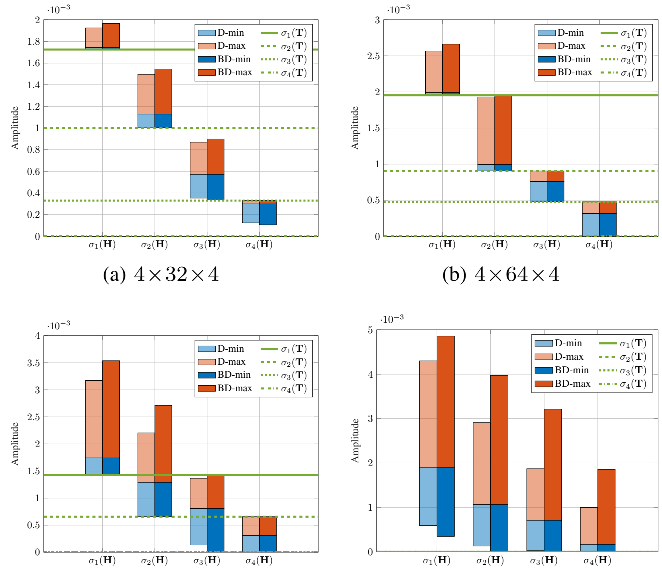

(a) $4 \times 32 \times 4$ (b) $4 \times 64 \times 4$

(c) $4 \times 128 \times 4$ (d) $4 \times 256 \times 4$

Fig. 3. Achievable channel singular values: analytical bounds (green lines) and optimized results (blue and red bars). 'D' means diagonal RIS and 'BD' means fully-connected BD-RIS.

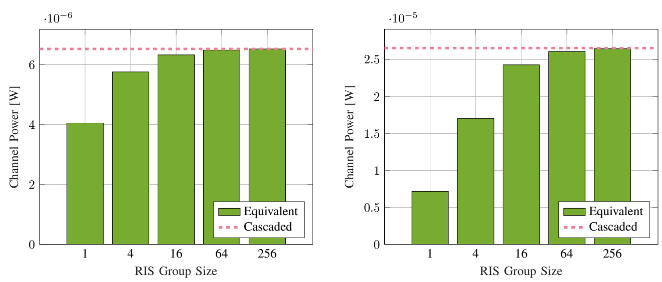

(a) $1 \times 256 \times 1$ (no direct) (b) $4 \times 256 \times 4$ (no direct)

Fig. 4. Average channel power versus BD-RIS group size and MIMO dimensions.

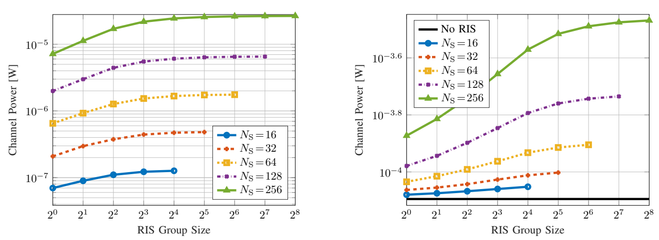

(a) $4 \times N_S \times 4$ (no direct) (b) $16 \times N_S \times 16$

Fig. 5. Average channel power versus antenna size and BD-RIS group size.

[2] Q. Wu and R. Zhang, "Intelligent reflecting surface enhanced wireless network via joint active and passive beamforming," *IEEE Transactions on Wireless Communications*, vol. 18, pp. 5394–5409, 11 2019. [Online]. Available: https://ieeexplore.ieee.org/document/8811733/

[3] ——, "Beamforming optimization for wireless network aided by intelligent reflecting surface with discrete phase shifts," *IEEE Transactions on Communications*, vol. 68, pp. 1838–1851, 3 2020. [Online]. Available: https://ieeexplore.ieee.org/document/8930608/

[4] Y. Yang, S. Zhang, and R. Zhang, "Irs-enhanced ofdma: Joint resource allocation and passive beamforming optimization," *IEEE Wireless Communications Letters*, vol. 9, pp. 760–764, 6 2020. [Online]. Available: https://ieeexplore.ieee.org/document/8964457/

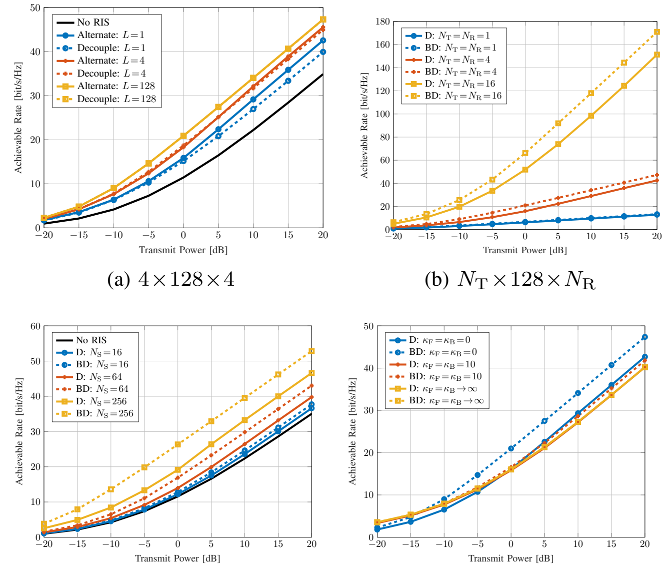

(a) $4 \times 128 \times 4$ (b) $N_T \times 128 \times N_R$

(c) $4 \times N_S \times 4$ (d) $4 \times 128 \times 4$

Fig. 6. Average channel power versus antenna size and BD-RIS group size.

[5] B. Zheng, C. You, and R. Zhang, "Double-irs assisted multi-user mimo: Cooperative passive beamforming design," *IEEE Transactions on Wireless Communications*, vol. 20, pp. 4513–4526, 7 2021. [Online]. Available: https://ieeexplore.ieee.org/document/9362274/

[6] X. Jia, J. Zhao, X. Zhou, and D. Niyato, "Intelligent reflecting surface-aided backscatter communications," vol. 2020-Janua. IEEE, 12 2020, pp. 1–6. [Online]. Available: https://ieeexplore.ieee.org/document/9348003/

[7] Y. C. Liang, Q. Zhang, J. Wang, R. Long, H. Zhou, and G. Yang, "Backscatter communication assisted by reconfigurable intelligent surfaces," *Proceedings of the IEEE*, 2022.

[8] R. Liu, M. Li, Y. Liu, Q. Wu, and Q. Liu, "Joint transmit waveform and passive beamforming design for ris-aided dfrc systems," *IEEE Journal of Selected Topics in Signal Processing*, pp. 1–1, 5 2022.

[9] M. Hua, Q. Wu, C. He, S. Ma, and W. Chen, "Joint active and passive beamforming design for irs-aided radar-communication," *IEEE Transactions on Wireless Communications*, vol. 22, pp. 2278–2294, 4 2023.

[10] Q. Wu, X. Zhou, W. Chen, J. Li, and X. Zhang, "Irs-aided wpcns: A new optimization framework for dynamic irs beamforming," *IEEE Transactions on Wireless Communications*, pp. 1–1, 12 2021.

[11] Z. Feng, B. Clerckx, and Y. Zhao, "Waveform and beamforming design for intelligent reflecting surface aided wireless power transfer: Single-user and multi-user solutions," *IEEE Transactions on Wireless Communications*, 2022.

[12] Y. Zhao, B. Clerckx, and Z. Feng, "Irs-aided swipt: Joint waveform, active and passive beamforming design under nonlinear harvester model," *IEEE Transactions on Communications*, vol. 70, pp. 1345–1359, 2022.

[13] R. Karasik, O. Simeone, M. D. Renzo, and S. S. Shitz, "Beyond max-snr: Joint encoding for reconfigurable intelligent surfaces," vol. 2020-June. IEEE, 6 2020, pp. 2965–2970. [Online]. Available: https://ieeexplore.ieee.org/document/9174060/

[14] E. Basar, "Reconfigurable intelligent surface-based index modulation: A new beyond mimo paradigm for 6g," *IEEE Transactions on Communications*, vol. 68, pp. 3187–3196, 5 2020. [Online]. Available: https://ieeexplore.ieee.org/document/8981888/

[15] Y. Zhao and B. Clerckx, "Riscatter: Unifying backscatter communication and reconfigurable intelligent surface," 12 2022. [Online]. Available: http://arxiv.org/abs/2212.09121

[16] W. Tang, J. Y. Dai, M. Chen, X. Li, Q. Cheng, S. Jin, K. Wong, and T. J. Cui, "Programmable metasurface-based rf chain-free 8psk wireless transmitter," *Electronics Letters*, vol. 55, pp. 417–420, 4 2019. [Online]. Available: https://onlinelibrary.wiley.com/doi/10.1049/el.2019.0400

[17] J. Y. Dai, W. Tang, L. X. Yang, X. Li, M. Z. Chen, J. C. Ke, Q. Cheng, S. Jin, and T. J. Cui, "Realization of multi-modulation schemes for wireless communication by time-domain digital coding metasurface," *IEEE Transactions on Antennas and Propagation*, vol. 68, pp. 1618–1627, 3 2020. [Online]. Available: https://ieeexplore.ieee.org/document/8901437/

[18] Q. Wu and R. Zhang, “Towards smart and reconfigurable environment: Intelligent reflecting surface aided wireless network,” *IEEE Communications Magazine*, vol. 58, pp. 106–112, 1 2020. [Online]. Available: https://ieeexplore.ieee.org/document/8910627/

[19] S. Shen, B. Clerckx, and R. Murch, “Modeling and architecture design of reconfigurable intelligent surfaces using scattering parameter network analysis,” *IEEE Transactions on Wireless Communications*, pp. 1–1, 11 2021. [Online]. Available: https://ieeexplore.ieee.org/document/9514409/

[20] H. Li, S. Shen, and B. Clerckx, “Beyond diagonal reconfigurable intelligent surfaces: From transmitting and reflecting modes to single-, group-, and fully-connected architectures,” *IEEE Transactions on Wireless Communications*, vol. 22, pp. 2311–2324, 4 2023.

[21] M. Nerini, S. Shen, and B. Clerckx, “Closed-form global optimization of beyond diagonal reconfigurable intelligent surfaces,” *IEEE Transactions on Wireless Communications*, pp. 1–1, 2023. [Online]. Available: https://ieeexplore.ieee.org/document/10155675/

[22] I. Santamaria, M. Soleymani, E. Jorswieck, and J. Gutiérrez, “Snr maximization in beyond diagonal ris-assisted single and multiple antenna links,” *IEEE Signal Processing Letters*, vol. 30, pp. 923–926, 2023. [Online]. Available: https://ieeexplore.ieee.org/document/10187688/

[23] T. Fang and Y. Mao, “A low-complexity beamforming design for beyond-diagonal ris aided multi-user networks,” *IEEE Communications Letters*, pp. 1–1, 7 2023. [Online]. Available: https://ieeexplore.ieee.org/document/10319662/

[24] M. Nerini, S. Shen, H. Li, and B. Clerckx, “Beyond diagonal reconfigurable intelligent surfaces utilizing graph theory: Modeling, architecture design, and optimization,” 5 2023. [Online]. Available: http://arxiv.org/abs/2305.05013

[25] Y. Zhou, Y. Liu, H. Li, Q. Wu, S. Shen, and B. Clerckx, “Optimizing power consumption, energy efficiency and sum-rate using beyond diagonal ris — a unified approach,” *IEEE Transactions on Wireless Communications*, pp. 1–1, 2023. [Online]. Available: https://ieeexplore.ieee.org/document/10364738/

[26] H. Li, S. Shen, and B. Clerckx, “A dynamic grouping strategy for beyond diagonal reconfigurable intelligent surfaces with hybrid transmitting and reflecting mode,” *IEEE Transactions on Vehicular Technology*, 12 2023.

[27] G. Bartoli, A. Abrardo, N. Decarli, D. Dardari, and M. D. Renzo, “Spatial multiplexing in near field mimo channels with reconfigurable intelligent surfaces,” *IET Signal Processing*, vol. 17, 3 2023. [Online]. Available: https://ietresearch.onlinelibrary.wiley.com/doi/10.1049/sil2.12195

[28] H. Li, S. Shen, and B. Clerckx, “Beyond diagonal reconfigurable intelligent surfaces: A multi-sector mode enabling highly directional full-space wireless coverage,” *IEEE Journal on Selected Areas in Communications*, vol. 41, pp. 2446–2460, 8 2023.

[29] H. Li, Y. Zhang, and B. Clerckx, “Channel estimation for beyond diagonal reconfigurable intelligent surfaces with group-connected architectures,” 7 2023. [Online]. Available: http://arxiv.org/abs/2307.06129

[30] H. Li, S. Shen, M. Nerini, M. D. Renzo, and B. Clerckx, “Beyond diagonal reconfigurable intelligent surfaces with mutual coupling: Modeling and optimization,” 10 2023. [Online]. Available: http://arxiv.org/abs/2310.02708

[31] H. Li, S. Shen, M. Nerini, and B. Clerckx, “Reconfigurable intelligent surfaces 2.0: Beyond diagonal phase shift matrices,” 1 2023. [Online]. Available: http://arxiv.org/abs/2301.03288

[32] B. Ning, Z. Chen, W. Chen, and J. Fang, “Beamforming optimization for intelligent reflecting surface assisted mimo: A sum-path-gain maximization approach,” *IEEE Wireless Communications Letters*, vol. 9, pp. 1105–1109, 7 2020.

[33] O. Ozdogan, E. Bjornson, and E. G. Larsson, “Using intelligent reflecting surfaces for rank improvement in mimo communications.” IEEE, 5 2020, pp. 9160–9164. [Online]. Available: https://ieeexplore.ieee.org/document/9052904/

[34] G.-H. Li, D.-W. Yue, and S.-N. Jin, “Spatially correlated rayleigh fading characteristics of ris-aided mmwave mimo communications,” *IEEE Communications Letters*, vol. 27, pp. 2222–2226, 8 2023. [Online]. Available: https://ieeexplore.ieee.org/document/10164200/

[35] Y. Zheng, T. Lin, and Y. Zhu, “Passive beamforming for irs-assisted mu-mimo systems with one-bit adcs: An ser minimization design approach,” *IEEE Communications Letters*, vol. 26, pp. 1101–1105, 5 2022. [Online]. Available: https://ieeexplore.ieee.org/document/9706177/

[36] W. Huang, B. Lei, S. He, C. Kai, and C. Li, “Condition number improvement of irs-aided near-field mimo channels.” IEEE, 5 2023, pp. 1210–1215. [Online]. Available: https://ieeexplore.ieee.org/document/10283534/

[37] M. A. ElMossallamy, H. Zhang, R. Sultan, K. G. Seddik, L. Song, G. Y. Li, and Z. Han, “On spatial multiplexing using reconfigurable intelligent surfaces,” *IEEE Wireless Communications Letters*, vol. 10, pp. 226–230, 2 2021. [Online]. Available: https://ieeexplore.ieee.org/document/9200661/

[38] S. Meng, W. Tang, W. Chen, J. Lan, Q. Y. Zhou, Y. Han, X. Li, and S. Jin, “Rank optimization for mimo channel with ris: Simulation and measurement,” 7 2023. [Online]. Available: http://arxiv.org/abs/2307.13237

[39] T. E. Abrudan, J. Eriksson, and V. Koivunen, “Steepest descent algorithms for optimization under unitary matrix constraint,” *IEEE Transactions on Signal Processing*, vol. 56, pp. 1134–1147, 3 2008. [Online]. Available: http://ieeexplore.ieee.org/document/4436033/

[40] T. Abrudan, J. Eriksson, and V. Koivunen, “Conjugate gradient algorithm for optimization under unitary matrix constraint,” *Signal Processing*, vol. 89, pp. 1704–1714, 9 2009. [Online]. Available: https://linkinghub.elsevier.com/retrieve/pii/S0165168409000814

[41] A. Edelman, T. A. Arias, and S. T. Smith, “The geometry of algorithms with orthogonality constraints,” *SIAM Journal on Matrix Analysis and Applications*, vol. 20, pp. 303–353, 1 1998. [Online]. Available: http://epubs.siam.org/doi/10.1137/S0895479895290954

[42] P.-A. Absil, R. Mahony, and R. Sepulchre, *Optimization Algorithms on Matrix Manifolds*. Princeton University Press, 2009. [Online]. Available: https://books.google.co.uk/books?id=NSQGQeLN3NcC

[43] C. Pan, G. Zhou, K. Zhi, S. Hong, T. Wu, Y. Pan, H. Ren, M. D. Renzo, A. L. Swindlehurst, R. Zhang, and A. Y. Zhang, “An overview of signal processing techniques for ris/irs-aided wireless systems,” *IEEE Journal of Selected Topics in Signal Processing*, vol. 16, pp. 883–917, 8 2022. [Online]. Available: https://ieeexplore.ieee.org/document/9847080/

[44] M. T. Ivrlac and J. A. Nossek, “Toward a circuit theory of communication,” *IEEE Transactions on Circuits and Systems I: Regular Papers*, vol. 57, pp. 1663–1683, 7 2010. [Online]. Available: https://ieeexplore.ieee.org/document/5446312/

[45] H.-R. Ahn, *Asymmetric Passive Components in Microwave Integrated Circuits*. Wiley, 2006. [Online]. Available: https://books.google.co.uk/books?id=X6WdLbOuSNQC

[46] E. Polak and G. Ribiere, “Note sur la convergence de méthodes de directions conjuguées,” *Revue française d'informatique et de recherche opérationnelle. Série rouge*, vol. 3, pp. 35–43, 1969.

[47] L. Armijo, “Minimization of functions having lipschitz continuous first partial derivatives,” *Pacific Journal of Mathematics*, vol. 16, pp. 1–3, 1 1966. [Online]. Available: http://msp.org/pjm/1966/16-1/p01.xhtml

[48] A. Hjorungnes and D. Gesbert, “Complex-valued matrix differentiation: Techniques and key results,” *IEEE Transactions on Signal Processing*, vol. 55, pp. 2740–2746, 6 2007. [Online]. Available: http://ieeexplore.ieee.org/document/4203075/

[49] G. H. Golub and C. F. V. Loan, *Matrix Computations*. Johns Hopkins University Press, 2013. [Online]. Available: https://jhupbooks.press.jhu.edu/title/matrix-computations

[50] D. Semmler, M. Joham, and W. Utschick, “High snr analysis of ris-aided mimo broadcast channels,” in *2023 IEEE 24th International Workshop on Signal Processing Advances in Wireless Communications (SPAWC)*. IEEE, 9 2023, pp. 221–225. [Online]. Available: https://ieeexplore.ieee.org/document/10304487/

[51] W. Fulton, “Eigenvalues, invariant factors, highest weights, and schubert calculus,” *Bulletin of the American Mathematical Society*, vol. 37, pp. 209–249, 4 2000. [Online]. Available: https://www.ams.org/bull/2000-37-03/S0273-0979-00-00865-X/

[52] B. Clerckx and C. Oestges, *MIMO Wireless Networks: Channels, Techniques and Standards for Multi-Antenna, Multi-User and Multi-Cell Systems*. Elsevier Science, 2013. [Online]. Available: https://books.google.co.uk/books?id=drEX1J7jHUIC

[53] J. C. Gower and G. B. Dijksterhuis, *Procrustes Problems*. OUP Oxford, 2004. [Online]. Available: https://books.google.co.uk/books?id=kRRREAAAQBAJ

[54] T. Bell, “Global positioning system-based attitude determination and the orthogonal procrustes problem,” *Journal of Guidance, Control, and Dynamics*, vol. 26, pp. 820–822, 9 2003. [Online]. Available: https://arc.aiaa.org/doi/10.2514/2.5117

[55] F. Nie, R. Zhang, and X. Li, “A generalized power iteration method for solving quadratic problem on the stiefel manifold,” *Science China Information Sciences*, vol. 60, p. 112101, 11 2017. [Online]. Available: http://link.springer.com/10.1007/s11432-016-9021-9